Carbon 156 (2020) 453–462

Contents lists available at ScienceDirect

Carbon

journal homepage: www.elsevier.com/locate/carbon

Laser-driven direct synthesis of carbon nanodots and application as sensitizers for visible-light photocatalysis

Nuria Mas [a, b], Jose L. Hueso [a, b, c], Gema Martinez [a, b, c, *], Ainhoa Madrid [a, b, c], Reyes Mallada [a, b, c], M. Carmen Ortega-Liebana [a, b], Carlos Bueno-Alejo [a, b], Jesus Santamaria [a, b, c, **]

[a] Institute of Nanoscience of Aragon (INA) and Department of Chemical and Environmental Engineering, Campus Rio Ebro, 50018, Zaragoza, Spain
[b] Networking Research Center on Bioengineering, Biomaterials and Nanomedicine (CIBER-BBN), 28029, Madrid, Spain
[c] Instituto de Ciencia de Materiales de Aragon (ICMA), Consejo Superior de Investigaciones Científicas (CSIC-Universidad de Zaragoza), Zaragoza, Spain

ARTICLE INFO

Article history:
Received 1 August 2019
Received in revised form
23 September 2019
Accepted 24 September 2019
Available online 25 September 2019

ABSTRACT

We present the first successful synthesis of monodisperse carbon nanodots (CNDs) with tunable photoluminescence (PL) carried out by laser pyrolysis of two common volatile organic precursors such as toluene and pyridine. Remarkably, the initial chemical composition of the precursor determines the formation of undoped or N-doped CNDs and their corresponding absorption response in the visible range (expanded for the latter). We demonstrate the control and versatility of this synthesis method to tune the final outcome and its potential to explore a great number of potential solvent candidates. Furthermore, we have successfully exploited these CNDs (both undoped and N-doped) as effective sensitizers of TiO_2 nanoparticles in the visible-light driven photo-degradation of a cationic dye selected as model organic pollutant.

1. Introduction

Luminescent carbon-based nanostructures such as graphene dots, carbon nanotubes (CNTs) or carbon nanodots (CNDs) have attracted much attention in recent years on account of their outstanding optical properties and potential applications [1–5]. Broad range optical response is strongly desirable in applications such as bioimaging, sensing, solar cells and theranostics [2,4,6–20]. Furthermore, their use as photosensitizers to expand the photocatalytic response of semiconductors beyond the UV range has also attracted a great attention in photocatalysis in the Advanced Oxidation Process (AOP) of organic pollutants present in wastewaters [2,4,11,20–41]. These features make CNDs an excellent alternative to semiconductor quantum dots (QDs) or up-converting rare-earth based nanoparticles (UCNPs) that are mostly based on scarce or potentially more toxic components. CNDs are typically synthesized by wet chemistry routes (i.e. microwave or hydrothermal methods), which provide high control of particle size distributions [6,22,35,42–44]. However, these methods normally demand extended reaction times and yield limited quantities. Furthermore, additional costly and tedious post-synthetic treatments are typically required due to the lack of chemical composition homogeneity [45–47]. Alternatively, CNDs have been also produced by laser driven methods involving either the laser ablation of solid target in organic solution [48–51], or alternatively the laser fragmentation of powdered carbon materials [51,52]. These routes constitute a single step strategy that does not require the use of external chemical agents, guarantying the high-purity of synthesized CNDs. However, these approaches, alike other top-down methods, generally face the major drawback of an intrinsically wide size distribution of the produced nanoparticles and low production efficiency [51,53]. For instance, classical laser fragmentation only leads to the reduction of almost half of the original powder carbon material [54,55]. Additionally, these methods display limited availability of control in stoichiometry requirements, making them very restricted processes for the synthesis of doped CNDs. Among the laser synthesis methods, laser

* Corresponding author. Institute of Nanoscience of Aragon (INA) and Department of Chemical and Environmental Engineering, Campus Rio Ebro, 50018, Zaragoza, Spain.
** Corresponding author. Institute of Nanoscience of Aragon (INA) and Department of Chemical and Environmental Engineering, Campus Rio Ebro, 50018, Zaragoza, Spain.
E-mail addresses: gemamar@unizar.es (G. Martinez), jesus.santamaria@unizar.es (J. Santamaria).

https://doi.org/10.1016/j.carbon.2019.09.073
0008-6223/

pyrolysis represents an elegant alternative for the one-pot synthesis of a wide variety of carbonaceous materials, including amorphous carbon materials, fullerenes, carbon black, carbides or even graphene powders. In the process of CO_2 laser pyrolysis [45,56–60] the reaction proceeds in-between the laser beam and the molecular flow of gaseous/vapors phase reactants. The resultant condensable products are generated at the interface. The process is based on the energy coupling between the laser light and the precursor's mixture. In case of no absorbing gas precursors an additional substance the so-called sensitizer, has to be introduced among the reactants [61]. Compared with other laser-driven approaches, the laser pyrolysis allows: (i) a well-defined interaction volume delimited by the radiation cross-section and the emerging gas flow; (ii) spatial uniformity of the reaction zone; (iii) highly localized and faster heating (leading to rapid nucleation) with faster quenching of the particles grow and (iv) versatile adjusting of process parameters to endow the nanoparticle with different composition and tailored properties. Although the use of a laser source represents an attractive alternative to conventional synthesis methods of CNDs (i. e. continuous production, potential scalability, low purification needs) [58–60,62], to date it has not been possible to retrieve them as freestanding and well-dispersed nanoparticles.

Herein we present, to the best of our knowledge, the first example of highly monodisperse undoped and N-doped CNDs with tuneable optical response synthesized by laser pyrolysis. Furthermore, we have tested these CNDs as sensitizers to extend the photocatalytic response of titania beyond the UV range [21,25–31,35,41] in the photodegradation of an organic dye [63–65]. Volatile organic solvents (toluene and pyridine) were selected as carbon precursors, whereas the generated nanoparticles after laser irradiation were collected in a liquid media to prevent coalescence events [45,56,57]. With this selection we aimed at evaluating the potential N-doping effects caused by the subtle modification of the chemical composition of the organic precursors (by introducing an N heteroatom). In this regard, the addition of co-reactants containing N, P or S atoms has been used to promote the sensitizing capabilities of CNDs in conventional (e.g. hydrothermal) synthesis [8] but not achieved before through laser-driven pyrolysis. In addition, we evaluate the predominant role of the generated CNDs as electron donors with capacity to expand the absorption of anatase towards the visible range.

2. Experimental

2.1. Chemicals

Toluene (99.7%), pyridine (99.8%), triethylene glycol (TREG, 99%), titanium(IV) oxide 99.8% anatase (<200 nm pseudo spherical nanopowders), crystal violet dye, terephthalic acid (TA), ethylenediaminetetraacetic acid disodium salt (ACS reagent, 99% EDTA-Na_2), 1-butanol (ACS reagent grade), quinine hemisulphate salt monohydrate (bioreagent, 98%) and ethanol with analytical purity grade were purchased from Sigma-Aldrich and used without any further purification.

2.2. Laser-driven synthesis of carbon nanodots (undoped CNDs and N-doped CNDs)

The synthesis of the CNDs was carried out by laser pyrolysis technology. The continuous gas flow reactor and the liquid collection system have been described elsewhere [45,56,57]. The first step was the optimization of the process parameters. In general, the most relevant process parameters governing the synthesis include working pressure, gas flow rates, concentration of the precursor in the reactant stream and laser intensity [45,56,57]. The overall operating pressure and the gas flow rates determine the time exposure in the laser beam. Both variables tend to shift the residence time in opposite direction. For instance, increasing the total pressure reduces the total volumetric flow rate and consequently increases the residence time (provided that the rest of parameters are fixed). In addition to these two parameters, the precursor feeding temperature (in case of liquid precursors) determines the final concentration of precursor in the reactant stream. All these key variables control the formation of gas phase aggregates and the final nanoparticle sizes. On the other hand, the laser power and the gas sensitizer (i.e. SF_6) feeding flow rate directly correlate with the temperatures reached in the reaction zone. Increasing both parameters favor an overall increase of the reaction temperature. In order to avoid further contaminations derived from the partial decomposition of the sensitizer, it is important to keep as low as possible the gas sensitizer gas flow rates. The optimized reaction conditions used in this work are listed in Table S1 (see Supplementary Material). Toluene (in the case of the undoped CNDs) or pyridine (for N-doped CNDs) were selected as carbon precursors. Both liquid solvents fulfill the requirements and can be easily fed into the reaction chamber due to their sufficiently high vapor pressure [66]. Moreover, the thermal process in which these precursor molecules are converted into atoms, releases C sp^2 (toluene) and C sp^2/N (pyridine), making them suitable candidates for the synthesis of carbon nanodots and further evaluation of the potential N-doping effects. The high temperature required for the decomposition of those precursors [67,68] led to use 250 W of laser power in order to reach the corresponding dissociation threshold, promoting at the same time the formation of highly crystalline undoped CNDs and N-doped CNDs. Lower laser power values typically yielded either amorphous or pseudo-crystalline carbonaceous networks. The volatile organic solvents were fed from a sealed glass vessel equipped with regulatory opening-close valves and immersed in a temperature-controlled bath. A flow rate of 30 sccm of sulfur hexafluoride (SF_6) selected as sensitizer that specifically absorbs the laser infrared wavelength, and 130 sccm of argon (Ar) was used as carrier gas passing through the organic precursor reservoir. An infrared CO_2 laser beam (Rofin SCx30, $\lambda = 10.6\ \mu m$) was settled to intersect orthogonally with the gas-phase organic reactant streams. The feeding inlet consisted of two concentric nozzles; the reactive gas flow (toluene/SF_6 or pyridine/SF_6) entered through the central inner tube (6.35 mm external diameter and 3.28 mm internal diameter), while an argon flow (coaxial gas) was fed through the external concentric tube (12.7 mm external diameter and 9.5 mm internal diameter). The coaxial argon stream (flow rate: 100 sccm) has the role of confining the reactant (precursor/SF_6 mixture) and the nucleated particles in a region close to the flow axis, minimizing deposition on the chamber walls. Additional Ar (600 sccm) and N_2 (200 sccm) streams were used to provide a protective sheath on the vertical and horizontal windows of the chamber. They also helped to avoid nanoparticle deposition onto the walls. All gas flow rates to the reactor were mass-flow controlled (Hytec). The working pressure in the reactor chamber was controlled through a diaphragm valve, located between the reaction chamber and the vacuum pump. The as-prepared nanoparticles were directly collected in a TREG container. Total reaction times were defined for 6 h. During the laser pyrolysis process, the TREG solution progressively darkened, as a clear signal of successful capture of the generated product materials. The resulting suspensions were labelled as CNDs and N-CNDs depending on the precursor used for their synthesis, toluene or pyridine, respectively. In order to carry out further characterization of the solids, the obtained suspension was rinsed with ethanol by centrifugation at 15000 rpm and 15 °C for 30 min to

remove the excess of TREG solvent. The resulting suspensions were stored at room temperature until further use. The synthesis of these nanomaterials has been performed by the Synthesis of Nanoparticles Unit of the ICTS "NANBIOSIS" at the Institute of Nanoscience of Aragon (INA)-Universidad de Zaragoza.

2.3. Carbon nanodots decorating TiO_2 nanoparticles

N-CNDs@TiO_2 nanohybrids were obtained via a drying-vacuum step at 90 °C. 0.2 g of TiO_2 anatase (which was previously heated treated at 180 °C during 2 h) were suspended in 2 mL of ethanol. Then 1 mL of N-CNDs suspended in ethanol was added. This suspension was stirred vigorously for 1 h at room temperature. After that the suspension was washed with water and centrifuged at 8000 rpm. The final solid was storaged after drying in a vacuum-driven oven at 90 °C during 1 h.

2.4. Characterization techniques

The morphologies and particle size distributions were determined by transmission electron microscopy (TEM) (FEI Tecnai T20, operating at 200 kV). The high-resolution TEM images were obtained in a Titan (FEI TITAN^3, operated at 300 kV and equipped with a Gatan Image Filter (GIF Tridiem 863)). To prepare the samples, the nanoparticle suspensions were diluted into deionized water and then dropcasted onto a holey carbon TEM grid. The surface chemical composition of CNDs was analyzed by X-ray photoelectron spectroscopy (XPS) with an Axis Ultra DLD (Kratos Tech.). A monochromatic Al Kα source (1486.6 eV) was employed with multiple runs at 12 kV, 10 mA and pass energy of 20 eV was used. The binding energies were calibrated to the internal C1s (284.3 eV) standard. Analyses of the peaks were performed with CasaXPS software, using a weighted sum of Lorentzian and Gaussian component curves after Shirley background subtraction as described previously in the literature [69–74]. Steady-state fluorescence emission spectra and photoluminescence excitation (PLE) survey spectra were collected on a JASCO FP-6500 spectrofluorometer equipped with a 450 W xenon lamp for excitation, with temperature controller ETC-273T at 25 °C, using 5 × 10 mm cuvettes and a LS55 Fluorescence Spectrometer (PerkinElmer) equipped with a xenon arc lamp as the light source and a quartz cell (10 × 10 mm). UV–Vis spectroscopy (V-67, Jasco Company) was used to analyze the absorbance spectra of the nanomaterials and the decoloration of crystal violet with a quartz cell of 1 cm light path. A 90 Plus Particle size analyzer (Brookhaven Instruments Corporation) was employed to determine ζ-potential measurements. The fluorescence quantum yields (QYs) were determined in aqueous solution using quinine sulphate (0.1 M in H_2SO_4) as reference fluorophore [6,75]. Using excitation wavelengths at 360 nm and keeping absorbance values below 0.1, QYs were 5% and 12% for undoped and N-doped CNDs, respectively and in line with previously reported carbon dots [20,35,76–78]. The surface morphology and Z-heights of the CNDs was characterized by atomic force microscopy (AFM) using a MultiMode 8 AFM system (Bruker). Images were taken in tapping mode using a high-resolution force modulation "Golden" silicon cantilevers (FMG01 series) with integrated tetrahedral tip, exhibiting a typical force constant and a resonant frequency of 3 N m^{-1} and 60 kHz, respectively. Raman characterization was carried out using a Raman Spectrometer WiTec alpha 300. A Nd:YAG laser operating at 532 nm laser was used for excitation of the Raman signal and the laser power for each sample was 1 mW. A 50x optical aperture was used resulting in a 1.2 μm diameter spot. Acquisition times of 1 s and a single spectrum accumulation per spectrum were typically required. Raman fitting of the raw spectra was carried out using 4 bands denoted as G, D, D″ and I following the convention established in previous literature [79–81] to establish the specific contributions of ordered and disordered fractions of the carbon network.

2.5. Photocatalytic degradation of crystal violet under white-LED irradiation

Photo-catalytic degradation assays of the cationic organic dye crystal violet (CV) were performed under white light LED irradiation. A white light LED emitter from LED-Engin (9.37 W, LZ4 model) was coupled to Synjet® a cooling system. The degradation assays were carried out suspending 0.6 mg of the TiO_2 decorated with the different CNDs or plain TiO_2 nanoparticles as control, in 3 mL of 0.025 mM Crystal Violet solution at its natural operating pH (pH = 6) [63–65,82]. The selection of this cationic dye was suitable due to the negative surface charge measured for the N-CNDs@TiO_2 nanoparticles by ζ-potential at that specific pH value. This charge differences would in principle favor a stronger electrostatic interaction between the photocatalyst and the organic molecule. The suspensions were magnetically stirred under dark for 30 min, prior to the irradiation with a white light emitting LED, in order to guarantee the establishment of an adsorption/desorption equilibrium. Different aliquots of 200 μL were taken at different time intervals. After centrifugation, the samples were measured by UV–visible spectroscopy monitoring the maximum absorbance of CV centred at 588 nm. All the photodegradation assays of CV were performed under the same experimental conditions. At least three assays were carried out for each tested solid and different N-CNDs@TiO_2 batches were tested in order to certify the reproducibility of the photocatalytic effect depending on the synthesized material.

2.6. Detection of radicals and quenching experiments under LED irradiation

The generation of hydroxyl radical under white LED irradiation was evaluated using disodium terephtalate (NaTA) as a probe, which selectively reacts with •OH to form a fluorescent derivative [35,78,83]. In a typical procedure, the detection of hydroxyl radicals (•OH) was carried out with the aid of disodium terephtalate (NaTA) (3 mL, 5 mM), which selectively reacts to generate a fluorescent product (2-hydroxyl disodium terephtalate) emitting at ca. 425 nm. After white LED illumination at different time intervals, the mixture solution was centrifuged to remove the photocatalyst nanoparticles. The fluorescence emission spectrum of the generated 2-hydroxy disodium terephtalate in the supernatant was subsequently measured at an excitation wavelength of 315 nm. The quenching experiments of the photocatalytic activity were carried out by degradation of CV under white LED light irradiation. 0.6 mg nanohybrids were suspended in 3 mL that contained 0.025 mM CV and 1 mM of EDTA-Na_2 (selected as hole scavenger) or alternatively 1 mM 1-butanol (as hydroxyl radical scavenger) in an aqueous suspension at pH 6. The suspensions were magnetically stirred under dark for 30 min, prior to the irradiation with one white light emitting LED, in order to guarantee the establishment of an adsorption/desorption equilibrium. Different aliquots of 200 μL were taken at several selected time intervals and after centrifugation of the samples these were measured in UV–visible spectroscopy equipment, following the decreasing of the maximum absorption peak of the dye centred at 588 nm.

3. Results and discussion

3.1. Synthesis and characterization of undoped and N-doped carbon dots retrieved by laser pyrolysis of different organic volatile solvents

Scheme 1 summarizes the laser pyrolysis process used to

generate the CNDs [45,56,57]. The resulting condensable products are generated from the laser induced chemical reaction at the interface of the laser beam and vaporized solvent (i. e. toluene for undoped or pyridine for N-doped CNDs). Sulfur hexafluoride is used as photosensitiser to accomplish the energy transfer process between the laser light and precursor's mixture. The net result of the laser excitation is a thermal process in which the reactant molecules are converted into atoms (Scheme 1 bottom, Reaction Zone). CNDs formation starts abruptly when a sufficient concentration of condensable products is reached in the vapor phase. To prepare small and spherical particles it is necessary to create a high degree of super-saturation for inducing the formation of a high density of nuclei and then quickly quench the particle growth by slowing down the kinetics, due to the fast decrease of temperature with radial distance. After leaving the hot reaction zone gas, the as-prepared nanoparticles are driven by the gas flow into the collector system containing TREG (Scheme 1 bottom, Collection System).

Transmission electron microscopy (TEM) analysis of the collected suspensions showed a narrow size distribution of nanoparticles with mean diameters of 2.3 ± 1.6 nm and 2.0 ± 0.7 nm for the CNDs derived from toluene (Fig. S1 and Fig. S2a) and pyridine (Fig. 1a and Fig. S2b), respectively. HR-TEM revealed that both CNDs are highly crystalline (Fig. 1a and b and Figs. S1a–S1b) stacked in a hexagonal crystal structure corresponding to graphite 2H with a space group P6_3mc [84,85]. These structures were confirmed on multiple individual CNDs by FFT images that rendered lattice

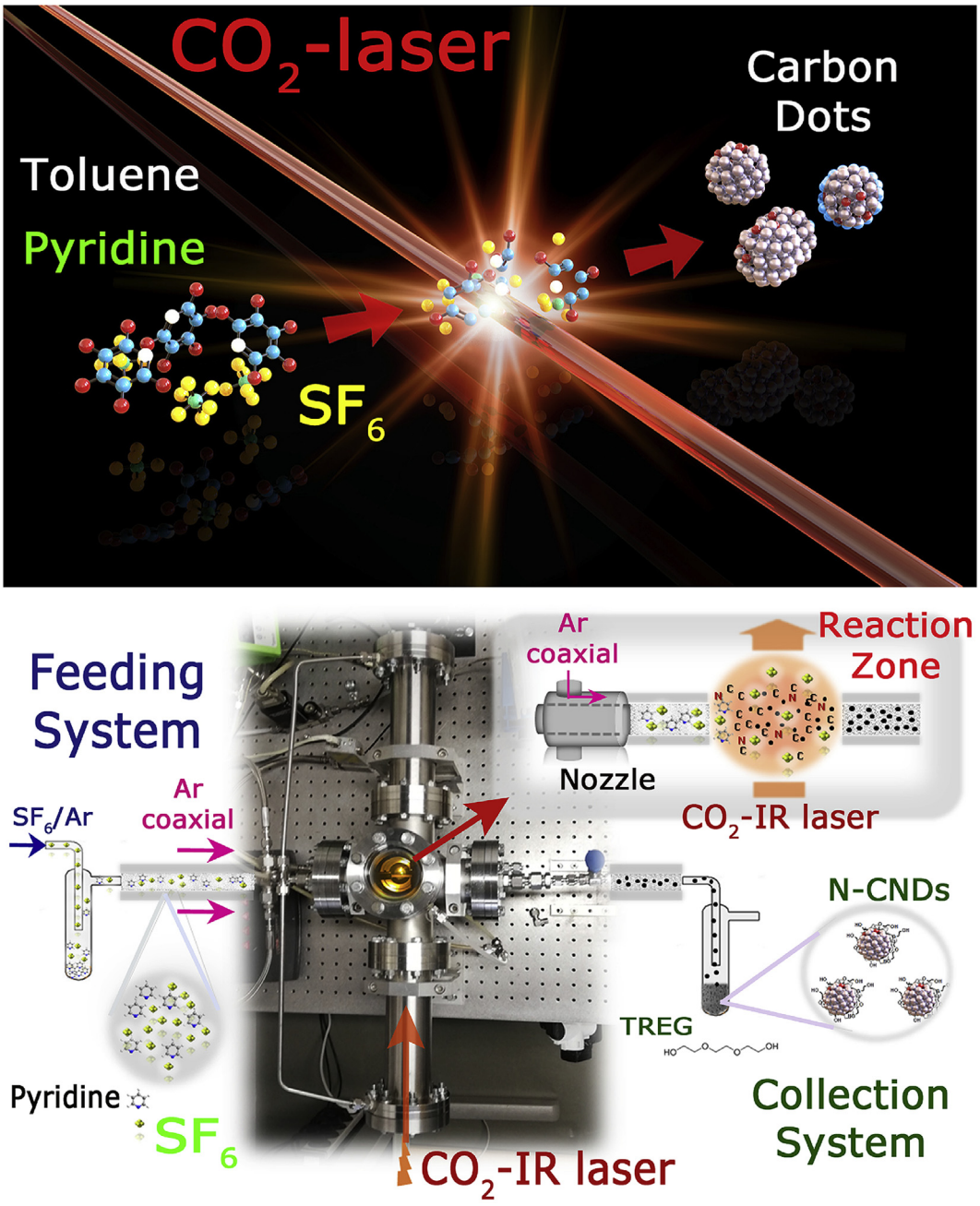

Scheme 1. (Top): Schematic display of the CO_2 laser assisted pyrolysis process to generate carbon nanodots derived from toluene or pyridine; (Bottom): Detailed scheme of the experimental setup including the feeding system, the reaction area and the collection in TREG medium.

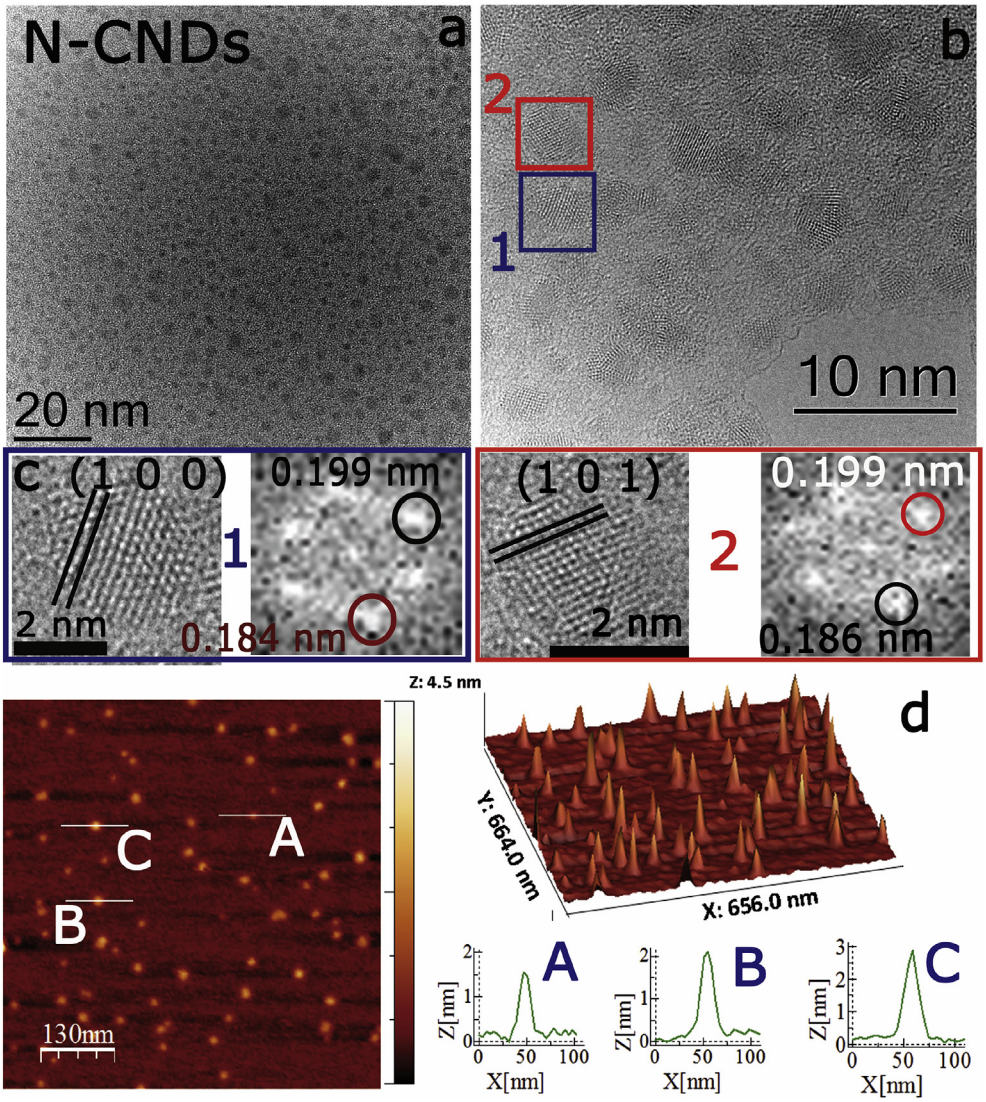

Fig. 1. Morphological characterization of the N-doped carbon nanodots (N-CNDs) retrieved from the laser-assisted pyrolysis of pyridine: a) Low-magnification TEM image accounting for the homogeneous distribution; b) HR-TEM image and c) insets accounting for the crystalline nature of the N-CNDs highlighted as 1,2 in b and their Fast Fourier Transform (FFT) images; d) 2D and 3D AFM topographic images including Z-height analysis at positions marked with blue lines and labelled as A-C in the 2D image of the N-CNDs. (A colour version of this figure can be viewed online.)

distances of 0.184 nm, 0.199 nm and 0.210 nm corresponding to (102), (101) and (100) planes of graphite 2H (see Fig. 1c and Fig. S1), respectively [84,85]. Given the two-dimensional nature of TEM, the shape of the CNDs was further assessed by Atomic Force Microscopy (AFM). Fig. 1d showed the 3D and 2D AFM topographic images of the N-doped CNDs. The location of A, B, and C were randomly spotted dots, their heights were 1.5, 2.1 and 2.9 nm, respectively, yielding and average height of 2.2 nm, which is close to the size (2.0 nm) obtained from TEM. An analogous dimension organization was observed in the case of the undoped CNDs (Fig. S3) and confirmed the pseudo-spherical distribution of the CNDs.

Representative first-order Raman spectra revealed two maxima for both CNDs centered at ~1350 cm^{-1} and ~1595 cm^{-1}, respectively (see Fig. S4). The additional broadening observed for the N-doped CNDs was mostly caused by an asymmetric tailing at lower shift values. The spectra were deconvoluted following previous fitting parameters by Maldonado et al. [80] or Cuesta et al. [79]. The fitting bands were referred to as G, D″, D and I, respectively. The G band at 1595 cm^{-1} arising from vibrational mode of ordered graphitic crystal planes with sp^2 bonds was only slightly more intense for the N-CNDs than the undoped ones (Fig. S4) and accounted for a similar level of ordered graphitic domains. In contrast, the contributions of D and especially D″ and I bands that are attributed to relaxations in local symmetry of graphitic planes caused by local distortions, stacking faults, the presence of impurities or the presence of disordered graphitic planes is more prominent in the Raman spectra recorded for the N-doped CNDs (Fig. S4) [79–81,86]. An analogous evolution has been previously observed in N-doped CNTs with increasing N levels [80].

Moreover, the N-doping was confirmed by XPS analysis (Fig. 2, Figs. S5–S6). The presence of N1s signal further confirmed the formation of N–C bonds in the carbon nanoparticles retrieved from pyridine (Fig. 2b). In contrast, the CNDs from toluene rendered no signal in this region (Fig. S5). N1s photoemission spectrum in the N-CNDs was fitted with two characteristics peaks (Fig. 2b). The first contribution at 399.4 eV was attributed to pyridinic-N (N-6), while the second centered at 401.7 eV was assigned to graphitic-N

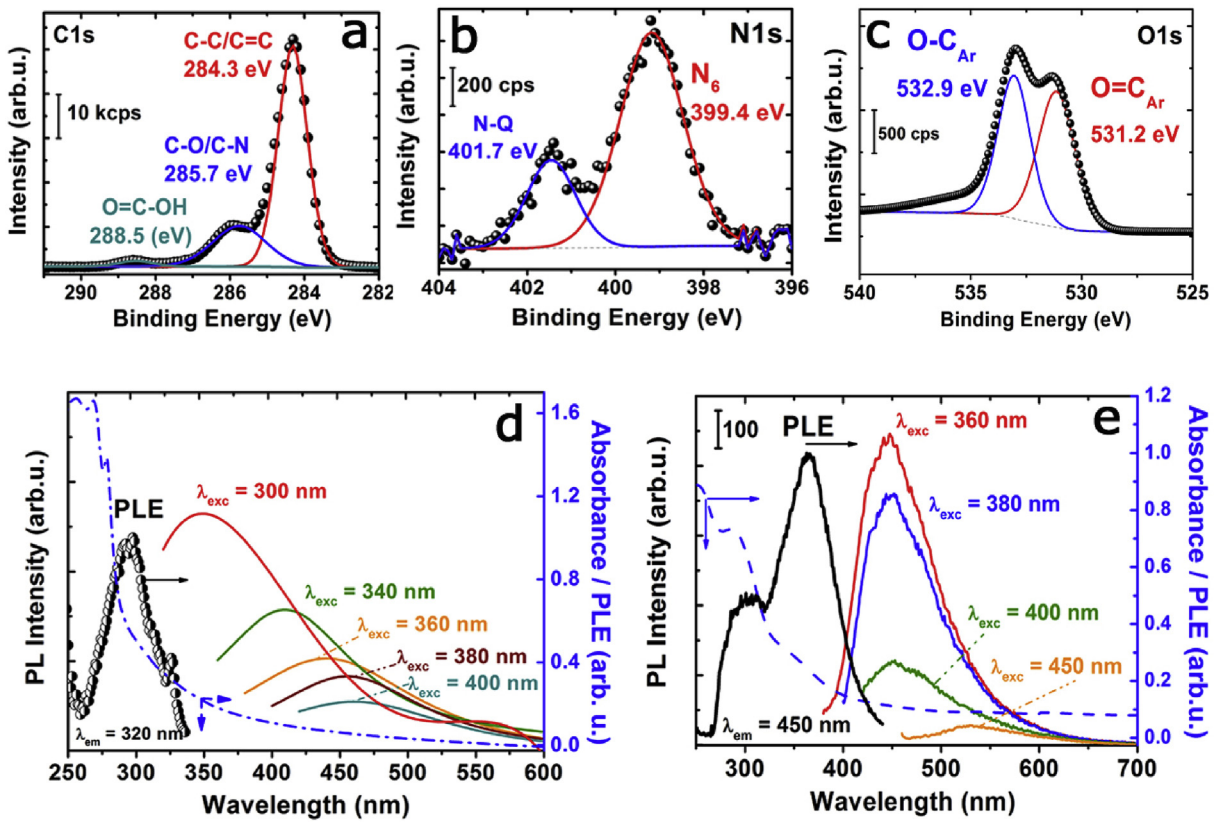

Fig. 2. X-ray photoemission spectra and fittings of the a) C1s region; b) N1s region; c) O1s region corresponding to the N-CNDs; d) Optical characterization of the undoped CNDs from toluene: Absorption spectrum, (blue dashed line), photoluminescence excitation spectrum at $\lambda_{em} = 320$ nm (PLE-black dotted curve) combined with the photoluminescence (PL) spectra for a range of excitation wavelengths (300–400 nm); e) Optical characterization of the N-doped CNDs from pyridine: Absorption spectrum (blue dashed line), photoluminescence excitation spectrum at $\lambda_{em} = 450$ nm (PLE-black curve) combined with the photoluminescence (PL) spectra for a range of excitation wavelengths (360–450 nm). (A colour version of this figure can be viewed online.)

quaternary amines (N-Q) (Fig. 2b) [13,16,17,26,70,72–75,83,87]. The surface atomic percentage detected for N was slightly above 1% (Table S2), thereby accounting for a limited doping level for the N-CNDs. In the expanded C1s spectrum of N-CNDs (Fig. 2a) the dominant peak at 284.3 eV raised from C–C bond with sp^2 hybridization, while the peaks at around 285.7, and 288.5 eV are attributed to C–N/C–O, and C=O and/or C=N bonds, respectively [69,70,75,87,88]. As expected, when N atoms are intercalated within the graphitic lattices the signals in the spectrum of C1s changed accordingly. Therefore, a less pronounced peak at 286.2 eV (C–O) was observed for the CNDs derived from toluene (Fig. S6). Analogous expanded O1s XP spectra were found for both type of carbon dots (Fig. 2c and Fig. S6). The O1s peaks at 531.3 and 532.9 eV shown in Fig. 2c were associated with oxygen doubly and singly bound to aromatic rings, respectively [13,69,71,72,74]. The major presence of surface oxygen in the N-doped CNDs (Table S2) points out to a major presence of carbon with defects containing surface active groups in accordance with the major disorder level detected by Raman spectroscopy (Fig. S4). The contribution of oxygen can be tentatively attributed with the oxygen present in the solvent precursors. Finally, it is worth mentioning the minor presence of S and F induced by the partial decomposition of the sensitizer (Table S2).

The absorption spectrum of the CNDs showed the typical π-π^* transition band at 250–275 nm [26] while in the N-doped CNDs a shoulder at 350 nm is typically assigned to the n-π^* transitions of the N centers (Fig. 2d and e) [1,25,26]. The broad absorption in the visible range has been previously attributed to a wider distribution of N levels and/or the presence of oxygen functional groups present in surface defects [5,16,20,26,31,47,76,85,89,90]. Therefore, in our case the doping with N atoms seems to disrupt the graphitic ordering in the CNDs and contributes to the creation of major fraction of disordered $sp^2 - sp^3$ clusters within the main graphitic network. This hypothesis has been further supported by XPS and Raman analysis (*vide supra*) and in previous works in the recent literature [16,28,31,91–94]. The evaluation of the optical properties corroborated the excitation wavelength dependence on the photoluminescence (PL) emission properties for the undoped CNDs (Fig. 2d) that is tentatively attributed to optical selection of differently sized nanoparticles (quantum effect), surface traps and/or reorganization of solvent's polarization [95]. In the case of N-CNDs such dependence is not observed (Fig. 2e), suggesting a different electronic configuration in which the radiative decay of excited electrons occur from N energy states of the N-CNDs [24–26], due to the relatively strong electron affinity of N atoms. Indeed, previous experimental observations and quantum-mechanical calculations have proved the strong electron-withdrawing ability of the N atoms within the conjugated C plane [24–26,96,97]. This is confirmed again with the photoluminescence excitation spectra (PLE) (Fig. 2e) in which the major contribution come from the wavelength corresponding to the n-π^* transitions at 350 nm in contrast with the corresponding excitation spectrum of the undoped CNDs where the major contribution comes from the π-π^* (Fig. 2d). This illustrates, to the best of our knowledge, the first examples of freestanding CNDs synthesized through the laser-assisted pyrolysis of regular solvents and how a minimal variation on the chemical structure of these starting precursors can be crucial to tune the optical response of the resulting products.

As an example of the functionality afforded by the CNDs, they have been applied in expanded-range photocatalysis. Taking into account that carbon nanostructures have been previously reported as successful sensitizers to expand the response of TiO_2 beyond the UV region [27–30,98–100], we used impregnation followed by drying under vacuum to deposit the undoped and N-doped CNDs onto commercial anatase nanoparticles (Fig. 3a) [21]. HRTEM analysis confirmed the homogeneous distribution of the N-CNDs onto the semiconductor phase (Fig. 3b). Likewise, an enhanced absorption towards the visible-NIR range was also observed by UV–Vis spectroscopy following the deposition of N-CNDs on anatase nanoparticles (Fig. 3c). This is attributable to the contribution of extra n-π^* transitions provided by the additional N energy surface states that will contribute to narrow the band gap of the hybrid material [25,26].

3.2. Evaluation of the carbon dots as visible-light photo-sensitizers

The visible-light driven photo-activity of plain anatase nanoparticles, CND-TiO_2 and N-CND-TiO_2 hybrids was evaluated in the degradation of an organic model dye such as crystal violet (CV) subjected to illumination with a high intensity white-light emitting LED (see Experimental section for details). As previously stated in the Experimental section, the photodegradation experiments were carried out at pH = 6, as typically reported for CV [63–65,82]. The ζ-Potential for the N-CNDs@TiO_2 nanoparticles at pH 6 (negatively charged, see Fig. S7) would be beneficial to ensure an optimal electrostatic interaction with the cationic dye. Fig. 3d shows the complete degradation of CV after 80 min of irradiation in the presence of the N-CNDs@TiO_2 photocatalyst. In contrast, the control experiment with no catalyst or the non-decorated TiO_2 support only rendered 10% and 40% maximum degradation, respectively under identical irradiation conditions. The hybrid containing the undoped CNDs achieved a maximum CV conversion of 50% after 80 min, thereby confirming the enhanced photodegradation capabilities of the N-CNDs (Fig. 3d).

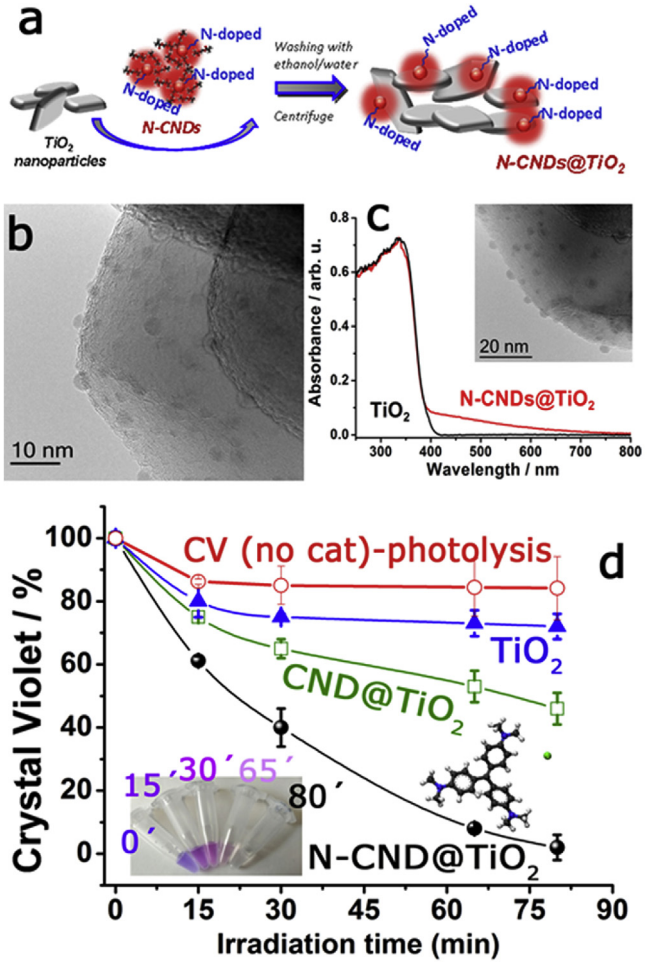

Fig. 3. a) Scheme representing the incorporation of the N-CNDs onto TiO_2 nanoparticles surface to obtain the final N-CNDs@TiO_2 hybrid nanomaterial; b) HR-TEM image of the carbon nanodots retrieved from pyridine (N-CNDs) after deployment onto the TiO_2 surface (N-CNDs@TiO_2); c) UV–visible absorbance spectra of TiO_2 powder nanoparticles with and without N-CNDs; d) Crystal violet photodegradation curves under white LED light irradiation, in the absence of catalyst (void circles), with TiO_2 nanoparticles (triangles) and in the presence of the undoped CNDs@TiO_2 (squared symbols) and N-CNDs@TiO_2 hybrids (filled circles), respectively. Inset: Crystal violet structure and digital pictures of different CV aliquots after irradiation at different time intervals in the presence of the N-CNDs@TiO_2 NPs.

Two additional consecutive photo-degradation experiments were carried out with the most active photocatalyst. After replacing with fresh dye solutions, the stability and reusability of the N-CNDs@TiO_2 were tested. There were no evidences of deactivation over three cycles (Fig. S8). In order to establish a mechanism, we studied the steady-state fluorescence changes of disodium terephthalate (NaTA) in the presence of the TiO_2 and N-CNDs@TiO_2 under white LED irradiation, respectively [35,78]. NaTA is a highly sensitive and selective fluorescent probe for hydroxyl radicals (•OH) (inset in Fig. 4a). The weakly fluorescent NaTA can react with •OH and convert into the highly fluorescent 2-hydroxy disodium terephtalate [33,35,83]. Preliminary control experiments evaluating the direct photolysis of NaTA under white LED irradiation or the potential catalytic effect of N-CNDs@TiO_2 in the absence of light were also carried out. No signal accounting for the generation of hydroxyl radicals was found (data not shown). Fig. 4 shows how the PL signal of hydroxylated NaTa byproduct is quite more prominent in the photocatalyst decorated with N-CNDs than in the plain TiO_2 NPs (Fig. 4a). This corroborates the enhanced radical generation under visible light exposure when N-CNDs are present as sensitizers. Additional experiments with the in situ generation of hydroxyl radicals under white LED light irradiation have been also monitored using disodium terephtalate (NaTA) as a probe, thereby corroborating the selective formation of these •OH radical groups only in the presence of the N-CNDs@TiO_2.

Additional experiments including different and specific scavengers (butanol for hydroxyl radicals and EDTA for holes) have been carried out in order to corroborate the active participation of these reactive oxidative species [101]. Given the much stronger quenching effect of EDTA (Fig. 4c), the mechanism seems to be preferentially driven by the photogeneration of holes. In our opinion, the presence of holes can be favored due to the strong interaction between the CNDs and the titania support that overlap their energy levels and facilitate a proper electron transfer from the excited levels of CNDs to the conduction band of TiO_2 (Fig. 4d) [24,27,102]. As a result, the electron-hole recombination rate in the CNDs is delayed and the holes can readily react with water molecules to form hydroxyl radicals ($h^+ + H_2O \rightarrow \bullet OH + H^+$, Fig. 4d), either on the surface of the CNDs or through the surface of Ti–O–Ti species as claimed by Nosaka et al. [103]. The other ROS formation mechanism governed by the interaction between photo-generated electrons and adsorbed oxygen molecules to yield oxygen superanions ($e- + O_2$ (ads) $\rightarrow \bullet O_2^- \rightarrow \ldots \rightarrow \bullet OH$, see Fig. 4d) is less straightforward and requires a major number of intermediate reactions to form the most reactive hydroxyl radicals [63,65]. It is also worth mentioning a small fraction of deep UV light from LED is also able to excite the TiO_2 itself (Figs. 3d and 4a). Still, the positive effect of both undoped and N-doped CNDs is clearly demonstrated (Fig. 3d).

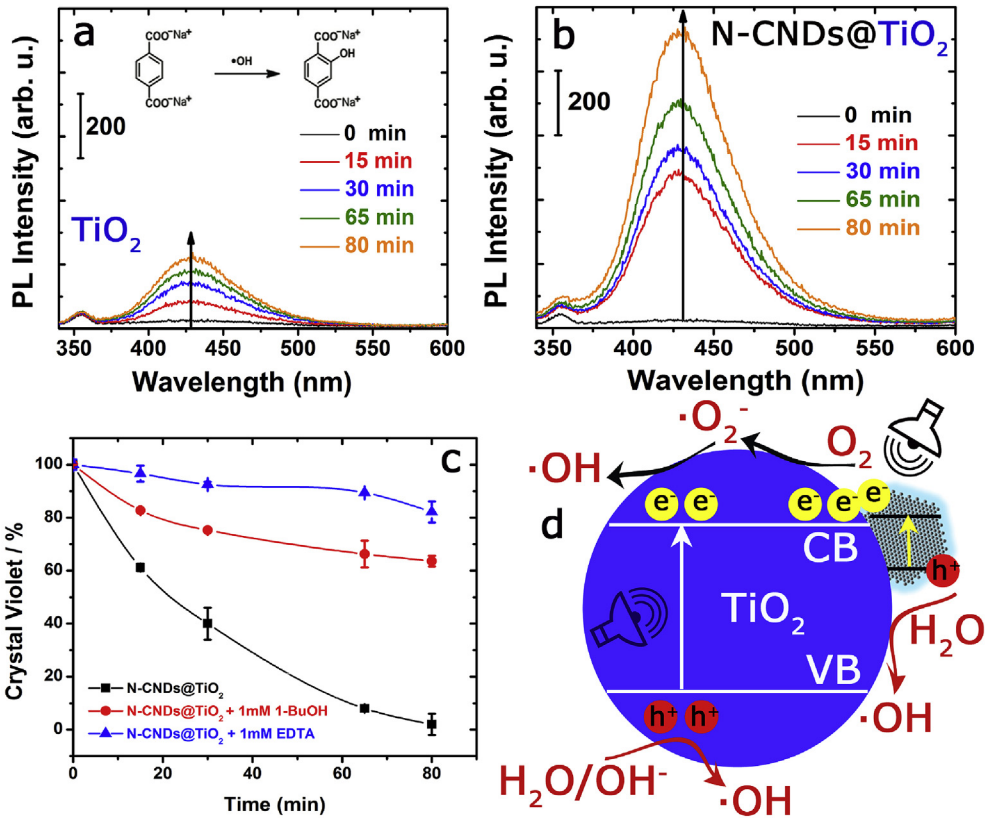

Fig. 4. Evaluation of the in situ generation of hydroxyl radicals upon photoirradiation with a high radiance white LED in the presence of a) plain anatase commercial nanoparticles and b) N-CNDs@TiO_2 nanohybrids; c) Quenching experiments to evaluate the influence of hole (EDTA) and hydroxyl radical (butanol) scavengers; d) Schematic display of the role of N-CNDs as photosensitizers able to withdraw electrons to the conduction band of the titania support and the main reaction pathways to form hydroxyl radicals.

4. Conclusions

In summary, for the first time we have shown that luminescent CNDs with tunable optical properties can be obtained through the laser-driven transformation of conventional organic solvents such as toluene and pyridine. Upon laser irradiation, the pyrolysis of toluene primarily led to the conformation of carbon nanodots with oxygen functional groups while the nitrogen-containing precursor gave rise to an N-doped carbon species with expanded optical range towards the visible range. The process is extremely fast and provides an optimal result, as the doping elements are intimately embedded in the carbon structures. This novel approach (laser-driven decomposition of organic molecules with the desired doping elements) harbours enormous prospects compared with classical preparation techniques for light-emitting CNDs, such as hydrothermal synthesis. In this case, the functionality of the carbon dots as efficient sensitizers to expand the photocatalytic response of anatase paves the way for multiple alternatives of synthesis where controlled doping with heteroatoms is relevant.

Competing financial interests

The authors declare no competing financial interests.

Declaration of competing interest

The authors declare that they have no known competing financial interests or personal relationships that could have appeared to influence the work reported in this paper.

Acknowledgements

Financial support from the European Research Council (ERC Advanced Grant CADENCE number 742684) is gratefully acknowledged. We also acknowledge the support from NANOLIGHT (REA grant number 294094), CIBER-BBN and MINECO (Spain) with project CTQ2016-79419-R. The synthesis of materials has been performed by the Platform of Production of Biomaterials and Nanoparticles of the NANOBIOSIS ICTS, more specifically by the Nanoparticle Synthesis Unit of the CIBER in Bioengineering, Biomaterials & Nanomedicine (CIBER-BBN). The TEM studies were conducted at the Laboratorio de Microscopias Avanzadas, Instituto de Nanociencia de Aragon, Universidad de Zaragoza, Spain. We thank Dr. Silvia Irusta for her help in the XPS measurements.

Appendix A. Supplementary data

Supplementary data to this article can be found online at https://doi.org/10.1016/j.carbon.2019.09.073.

References

[1] S.N. Baker, G.A. Baker, Luminescent carbon nanodots: emergent nanolights, Angew. Chem. Int. Ed. 49 (2010) 6726–6744.
[2] S.Y. Lim, W. Shen, Z.Q. Gao, Carbon quantum dots and their applications, Chem. Soc. Rev. 44 (2015) 362–381.
[3] C.M. Zhang, J. Lin, Defect-related luminescent materials: synthesis, emission properties and applications, Chem. Soc. Rev. 41 (2012) 7938–7961.
[4] Q.J. Xiang, J.G. Yu, M. Jaroniec, Graphene-based semiconductor photocatalysts, Chem. Soc. Rev. 41 (2012) 782–796.
[5] S.T. Yang, Y.S. Ho, Research performance and trends of fluorescent carbon nanoparticles: a science citation index expanded-based analysis, J. Nano Res. 21 (2019) 1–12.

[6] M.C. Ortega-Liebana, M.M. Encabo-Berzosa, M.J. Ruedas-Rama, J.L. Hueso, Nitrogen-induced transformation of vitamin C into multifunctional up-converting carbon nanodots in the visible-NIR range, Chem. Eur J. 23 (2017) 3067–3073.

[7] J.Y. Qin, J.P. Huo, P.Y. Zhang, J. Zeng, T.T. Wang, H.P. Zeng, Improving the photocatalytic hydrogen production of Ag/g-C_3N_4 nanocomposites by dye-sensitization under visible light irradiation, Nanoscale 8 (2016) 2249–2259.

[8] D. Qu, M. Zheng, P. Du, Y. Zhou, L.G. Zhang, D. Li, H.Q. Tan, Z. Zhao, Z.G. Xie, Z.C. Sun, Highly luminescent S, N co-doped graphene quantum dots with broad visible absorption bands for visible light photocatalysts, Nanoscale 5 (2013) 12272–12277.

[9] S.J. Zhu, Q.N. Meng, L. Wang, J.H. Zhang, Y.B. Song, H. Jin, K. Zhang, H.C. Sun, H.Y. Wang, B. Yang, Highly photoluminescent carbon dots for multicolor patterning, sensors, and bioimaging, Angew. Chem. Int. Ed. 52 (2013) 3953–3957.

[10] M.J. Ruedas-Rama, A. Orte, E.A.H. Hall, J.M. Alvarez-Pez, E.M. Talavera, Quantum dot photoluminescence lifetime-based pH nanosensor, Chem. Commun. 47 (2011) 2898–2900.

[11] X.T. Zheng, A. Ananthanarayanan, K.Q. Luo, P. Chen, Glowing graphene quantum dots and carbon dots: properties, syntheses, and biological applications, Small 11 (2015) 1620–1636.

[12] A.B. Bourlinos, A. Stassinopoulos, D. Anglos, R. Zboril, M. Karakassides, E.P. Giannelis, Surface functionalized carbogenic quantum dots, Small 4 (2008) 455–458.

[13] M.C. Ortega-Liebana, N.X. Chung, R. Limpens, L. Gomez, J.L. Hueso, J. Santamaria, T. Gregorkiewicz, Uniform luminescent carbon nanodots prepared by rapid pyrolysis of organic precursors confined within nanoporous templating structures, Carbon 117 (2017) 437–446.

[14] P. Roy, A.P. Periasamy, C.Y. Lin, G.M. Her, W.J. Chiu, C.L. Li, C.L. Shu, C.C. Huang, C.T. Liang, H.T. Chang, Photoluminescent graphene quantum dots for in vivo imaging of apoptotic cells, Nanoscale 7 (2015) 2504–2510.

[15] L.H. Shi, Y.Y. Li, X.F. Li, X.P. Wen, G.M. Zhang, J. Yang, C. Dong, S.M. Shuang, Facile and eco-friendly synthesis of green fluorescent carbon nanodots for applications in bioimaging, patterning and staining, Nanoscale 7 (2015) 7394–7401.

[16] K. Hola, M. Sudolska, S. Kalytchuk, D. Nachtigallova, A.L. Rogach, M. Otyepka, R. Zboril, Graphitic nitrogen triggers red fluorescence in carbon dots, ACS Nano 11 (2017) 12402–12410.

[17] K. Hola, Y. Zhang, Y. Wang, E.P. Giannelis, R. Zboril, A.L. Rogach, Carbon dots-Emerging light emitters for bioimaging, cancer therapy and optoelectronics, Nano Today 9 (2014) 590–603.

[18] C.J. Reckmeier, Y. Wang, R. Zboril, A.L. Rogach, Influence of doping and temperature on solvatochromic shifts in optical spectra of carbon dots, J. Phys. Chem. C 120 (2016) 10591–10604.

[19] Y. Xiong, J. Schneider, C.J. Reckmeier, H. Huang, P. Kasak, A.L. Rogach, Carbonization conditions influence the emission characteristics and the stability against photobleaching of nitrogen doped carbon dots, Nanoscale 9 (2017) 11730–11738.

[20] G.A.M. Hutton, B.C.M. Martindale, E. Reisner, Carbon dots as photosensitisers for solar-driven catalysis, Chem. Soc. Rev. 46 (2017) 6111–6123.

[21] M.C. Ortega-Liebana, J.L. Hueso, S. Ferdousi, R. Arenal, S. Irusta, K.L. Yeung, J. Santamaria, Extraordinary sensitizing effect of co-doped carbon nanodots derived from mate herb: application to enhanced photocatalytic degradation of chlorinated wastewater compounds under visible light, Appl. Catal. B Environ. 218 (2017) 68–79.

[22] D.H. Wang, L. Jia, X.L. Wu, L.Q. Lu, A.W. Xu, One-step hydrothermal synthesis of N-doped TiO_2/C nanocomposites with high visible light photocatalytic activity, Nanoscale 4 (2012) 576–584.

[23] M. Shamsipur, A. Barati, S. Karami, Long-wavelength, multicolor, and white-light emitting carbon-based dots: achievements made, challenges remaining, and applications, Carbon 124 (2017) 429–472.

[24] Z.J. Zhang, T.T. Zheng, X.M. Li, J.Y. Xu, H.B. Zeng, Progress of carbon quantum dots in photocatalysis applications, Part. Part. Syst. Charact. 33 (2016) 457–472.

[25] R. Shi, Z. Li, H.J. Yu, L. Shang, C. Zhou, G.I.N. Waterhouse, L.Z. Wu, T.R. Zhang, Effect of nitrogen doping level on the performance of N-doped carbon quantum dot/TiO2 composites for photocatalytic hydrogen evolution, ChemSusChem 10 (2017) 4650–4656.

[26] Y.Q. Dong, H.C. Pang, H.B. Yang, C.X. Guo, J.W. Shao, Y.W. Chi, C.M. Li, T. Yu, Carbon-based dots Co-doped with nitrogen and sulfur for high quantum yield and excitation-independent emission, Angew. Chem. Int. Ed. 52 (2013) 7800–7804.

[27] V. Binas, D. Venieri, D. Kotzias, G. Kiriakidis, Modified TiO_2 based photocatalysts for improved air and health quality, J. Materiomics 3 (2017) 3–16.

[28] Y. Park, J. Yoo, B. Lim, W. Kwon, S.W. Rhee, Improving the functionality of carbon nanodots: doping and surface functionalization, J. Mater. Chem. 4 (2016) 11582–11603.

[29] N.R. Nalid, A. Majid, M.B. Tahir, N.A. Niaz, S. Khalid, Carbonaceous-TiO_2 nanomaterials for photocatalytic degradation of pollutants: a review, Ceram. Int. 43 (2017) 14552–14571.

[30] R. Leary, A. Westwood, Carbonaceous nanomaterials for the enhancement of TiO_2 photocatalysis, Carbon 49 (2011) 741–772.

[31] M. Han, S.J. Zhu, S.Y. Lu, Y.B. Song, T.L. Feng, S.Y. Tao, J.J. Liu, B. Yang, Recent progress on the photocatalysis of carbon dots: classification, mechanism and applications, Nano Today 19 (2018) 201–218.

[32] V. Likodimos, Photonic crystal-assisted visible light activated TiO_2 photocatalysis, Appl. Catal. B Environ. 230 (2018) 269–303.

[33] M.C. Ortega-Liebana, J.L. Hueso, A. Larrea, V. Sebastiana, J. Santamaria, Feroxyhyte nanoflakes coupled to up-converting carbon nanodots: a highly active, magnetically recoverable, Fenton-like photocatalyst in the visible-NIR range, Chem. Commun. 51 (2015) 16625–16628.

[34] X.W. Wang, G.Z. Sun, P. Routh, D.H. Kim, W. Huang, P. Chen, Heteroatom-doped graphene materials: syntheses, properties and applications, Chem. Soc. Rev. 43 (2014) 7067–7098.

[35] M.C. Ortega-Liebana, J.L. Hueso, S. Ferdousi, K.L. Yeung, J. Santamaria, Nitrogen-doped luminescent carbon nanodots for optimal photo-generation of hydroxyl radicals and visible-light expanded photo-catalysis, Diam. Relat. Mater. 65 (2016) 176–182.

[36] A.P. Bhirud, S.D. Sathaye, R.P. Waichal, J.D. Ambekar, C.J. Park, B.B. Kale, In-situ preparation of N-TiO_2/graphene nanocomposite and its enhanced photocatalytic hydrogen production by H_2S splitting under solar light, Nanoscale 7 (2015) 5023–5034.

[37] H.T. Li, R.H. Liu, S.Y. Lian, Y. Liu, H. Huang, Z.H. Kang, Near-infrared light controlled photocatalytic activity of carbon quantum dots for highly selective oxidation reaction, Nanoscale 5 (2013) 3289–3297.

[38] M.B. Vasic, M.S. Randjelovic, M.Z. Momilovic, B.Z. Matovic, A.R. Zarubica, Degradation of crystal violet over heterogeneous TiO_2 -based catalysts: the effect of process parameters, Process. Appl. Ceram. 10 (2016) 189–198.

[39] Q.H. Yao, L.P. Lin, T.T. Zhao, X. Chen, Advances in preparation, physico-chemical properties and applications of heteroatom-doped graphene quantum dots, Prog. Chem. 27 (2015) 1523–1530.

[40] A. Hosseinnia, M. Keyanpour-Rad, M. Pazouki, Photo-catalytic degradation of organic dyes with different chromophores by synthesized nanosize TiO_2 particles, World Appl. Sci. J. 8 (2010) 1327–1332.

[41] C.C. Chen, W.H. Ma, J.C. Zhao, Semiconductor-mediated photodegradation of pollutants under visible-light irradiation, Chem. Soc. Rev. 39 (2010) 4206–4219.

[42] H.P. Liu, T. Ye, C.D. Mao, Fluorescent carbon nanoparticles derived from candle soot, Angew. Chem. Int. Ed. 46 (2007) 6473–6475.

[43] S.N. Qu, X.Y. Wang, Q.P. Lu, X.Y. Liu, L.J. Wang, A biocompatible fluorescent ink based on water-soluble luminescent carbon nanodots, Angew. Chem. Int. Ed. 51 (2012) 12215–12218.

[44] X.F. Jia, J. Li, E.K. Wang, One-pot green synthesis of optically pH-sensitive carbon dots with upconversion luminescence, Nanoscale 4 (2012) 5572–5575.

[45] G. Martinez, A. Malumbres, R. Mallada, J.L. Hueso, S. Irusta, O. Bomati-Miguel, J. Santamaria, Use of a polyol liquid collection medium to obtain ultrasmall magnetic nanoparticles by laser pyrolysis, Nanotechnology 23 (2012) 425605 (9 pp).

[46] B.S. Chen, F.M. Li, S.X. Li, W. Weng, H.X. Guo, T. Guo, X.Y. Zhang, Y.B. Chen, T.T. Huang, X.L. Hong, S.Y. You, Y.M. Lin, K.H. Zeng, S. Chen, Large scale synthesis of photoluminescent carbon nanodots and their application for bioimaging, Nanoscale 5 (2013) 1967–1971.

[47] W. Ding, Z.D. Wei, S.G. Chen, X.Q. Qi, T. Yang, J.S. Hu, D. Wang, L.J. Wan, S.F. Alvi, L. Li, Space-Confinement-induced synthesis of pyridinic- and pyrrolic-nitrogen-doped graphene for the catalysis of oxygen reduction, Angew. Chem. Int. Ed. 52 (2013) 11755–11759.

[48] J. Lin, Z.W. Peng, Y.Y. Liu, F. Ruiz-Zepeda, R.Q. Ye, E.L.G. Samuel, M.J. Yacaman, B.I. Yakobson, J.M. Tour, Laser-induced porous graphene films from commercial polymers, Nat. Commun. 5 (2014) 5714 (8pp).

[49] T.N. Lin, K.H. Chih, C.T. Yuan, J.L. Shen, C.A.J. Lin, W.R. Liu, Laser-ablation production of graphene oxide nanostructures: from ribbons to quantum dots, Nanoscale 7 (2015) 2708–2715.

[50] R.Q. Ye, Y. Chyan, J.B. Zhang, Y.L. Li, X. Han, C. Kittrell, J.M. Tour, Laser-induced graphene formation on wood, Adv. Mater. 29 (2017) 1702211 (7pp).

[51] D.S. Zhang, B. Goekce, S. Barcikowski, Laser synthesis and processing of colloids: fundamentals and applications, Chem. Rev. 117 (2017) 3990–4103.

[52] C. Donate-Buendia, R. Torres-Mendieta, A. Pyatenko, E. Falomir, M. Fernandez-Alonso, G. Minguez-Vega, Fabrication by laser irradiation in a continuous flow jet of carbon quantum dots for fluorescence imaging, ACS Omega 3 (2018) 2735–2742.

[53] V. Amendola, M. Meneghetti, What controls the composition and the structure of nanomaterials generated by laser ablation in liquid solution? Phys. Chem. Chem. Phys. 15 (2013) 3027–3046.

[54] S.L. Hu, K.Y. Niu, J. Sun, J. Yang, N.Q. Zhao, X.W. Du, One-step synthesis of fluorescent carbon nanoparticles by laser irradiation, J. Mater. Chem. 19 (2009) 484–488.

[55] X.Y. Li, H.Q. Wang, Y. Shimizu, A. Pyatenko, K. Kawaguchi, N. Koshizaki, Preparation of carbon quantum dots with tunable photoluminescence by rapid laser passivation in ordinary organic solvents, Chem. Commun. 47 (2011) 932–934.

[56] A. Malumbres, G. Martinez, R. Mallada, J.L. Hueso, O. Bomati-Miguel, J. Santamaria, Continuous production of iron-based nanocrystals by laser pyrolysis. Effect of operating variables on size, composition and magnetic response, Nanotechnology 24 (2013) 325603 (13 pp).

[57] A. Malumbres, G. Martinez, J.L. Hueso, J. Gracia, R. Mallada, A. Ibarra, J. Santamaria, Facile production of stable silicon nanoparticles: laser chemistry coupled to in situ stabilization via room temperature hydrosilylation, Nanoscale 7 (2015) 8566–8573.

[58] G. Martinez, A. Malumbres, A. Lopez, R. Mallada, J.L. Hueso, J. Santamaria,

Laser-assisted production of carbon-encapsulated Pt-Co alloy nanoparticles for preferential oxidation of carbon monoxide, 6-Art.487, Front. Chem. (2018), 10 pp.
[59] M.T. Swihart, Vapor-phase synthesis of nanoparticles, Curr. Opin. Colloid Interface Sci. 8 (2003) 127–133.
[60] A.A. Puretzky, D.B. Geohegan, X. Fan, S.J. Pennycook, Dynamics of single-wall carbon nanotube synthesis by laser vaporization, Appl. Phys. Mater. Sci. Process 70 (2000) 153–160.
[61] E. Borsella, S. Botti, L. Caneve, L. De Dominicisand, R. Fantoni, IR multiple-photon excitation of polyatomic molecules: a route towards nano-structures, Phys. Scr. 78 (2008).
[62] V. Sebastian, M. Arruebo, J. Santamaria, Reaction engineering strategies for the production of inorganic nanomaterials, Small 10 (2014) 835–853.
[63] Y. Liu, X.Z. Liu, D.Z. Lu, P.F. Fang, R. Xiong, J.H. Wei, C.X. Pan, Carbon deposited TiO_2-based nanosheets with enhanced adsorption ability and visible light photocatalytic activity, J. Mol. Catal. A Chem. 392 (2014) 208–215.
[64] S. Senthilkumaar, K. Porkodi, Heterogeneous photocatalytic decomposition of Crystal Violet in UV-illuminated sol-gel derived nanocrystalline TiO_2 suspensions, J. Colloid Interface Sci. 288 (2005) 184–189.
[65] C.C. Chen, F.D. Mai, K.T. Chen, C.W. Wu, C.S. Lu, Photocatalyzed N-de-methylation and degradation of crystal violet in titania dispersions under UV irradiation, Dyes Pigments 75 (2007) 434–442.
[66] D.R. Lide (Ed.), CRC Handbook of Chemistry and Physics, 84th ed., CRC Press LLC, Boca Raton, 2003.
[67] N.R. Hore, D.K. Russell, Radical pathways in the thermal decomposition of pyridine and diazines: a laser pyrolysis and semi-empirical study, J. Chem. Soc.-Perkin Trans. 2 (1998) 269–275.
[68] K.M. Pamidimukkala, R.D. Kern, M.R. Patel, H.C. Wei, J.H. Kiefer, High-Temperature pyrolysis of toluene, J. Phys. Chem. 91 (1987) 2148–2154.
[69] J.P. Boudou, J.I. Paredes, A. Cuesta, A. Martinez-Alonso, J.M.D. Tascon, Oxygen plasma modification of pitch-based isotropic carbon fibres, Carbon 41 (2003) 41–56.
[70] J.R. Pels, F. Kapteijn, J.A. Moulijn, Q. Zhu, K.M. Thomas, Evolution of nitrogen functionalities in carbonaceous materials during pyrolysis, Carbon 33 (1995) 1641–1653.
[71] C. Hontoria-Lucas, A.J. Lopez-Peinado, J.D.D. Lopez-Gonzalez, M.L. Rojas-Cervantes, R.M. Martin-Aranda, Study of oxygen-containing groups in a series of graphite oxides - physical and chemical characterization, Carbon 33 (1995) 1585–1592.
[72] S. Biniak, G. Szymanski, J. Siedlewski, A. Swiatkowski, The characterization of activated carbons with oxygen and nitrogen surface groups, Carbon 35 (1997) 1799–1810.
[73] P. Garcia, J.F. Espinal, C.S.M. de Lecea, F. Mondragon, Experimental characterization and molecular simulation of nitrogen complexes formed upon NO-char reaction at 270 degrees C in the presence of H_2O and O-2, Carbon 42 (2004) 1507–1515.
[74] J.L. Hueso, J.P. Espinos, A. Caballero, J. Cotrino, A.R. Gonzalez-Elipe, XPS investigation of the reaction of carbon with NO, O-2, N-2 and H_2O plasmas, Carbon 45 (2007) 89–96.
[75] M.C. Ortega-Liebana, M.M. Encabo-Berzosa, A. Casanova, M.D. Pereboom, J.O. Alda, J.L. Hueso, J. Santamaria, Upconverting carbon nanodots from ethylenediaminetetraacetic acid (EDTA) as near-infrared activated photo-theranostic agents, Chem. Eur J. 25 (2019) 5539–5546.
[76] G.A.M. Hutton, B. Reuillard, B.C.M. Martindale, C.A. Caputo, C.W.J. Lockwood, J.N. Butt, E. Reisner, Carbon dots as versatile photosensitizers for solar-driven catalysis with redox enzymes, J. Am. Chem. Soc. 138 (2016) 16722–16730.
[77] B.C.M. Martindale, G.A.M. Hutton, C.A. Caputo, E. Reisner, Solar hydrogen production using carbon quantum dots and a molecular nickel catalyst, J. Am. Chem. Soc. 137 (2015) 6018–6025.
[78] M.C. Ortega-Liebana, J.L. Hueso, R. Arenal, J. Santamaria, Titania-coated gold nanorods with expanded photocatalytic response. Enzyme-like glucose oxidation under near-infrared illumination, Nanoscale 9 (2017) 1787–1792.
[79] A. Cuesta, P. Dhamelincourt, J. Laureyns, A. Martinezalonso, J.M.D. Tascon, Raman microprobe studies on carbon materials, Carbon 32 (1994) 1523–1532.
[80] S. Maldonado, S. Morin, K.J. Stevenson, Structure, composition, and chemical reactivity of carbon nanotubes by selective nitrogen doping, Carbon 44 (2006) 1429–1437.
[81] A.P. del Pino, A.M. Villarroya, A. Chuquitarqui, C. Logofatu, D. Tonti, E. Gyorgy, Reactive laser synthesis of nitrogen-doped hybrid graphene-based electrodes for energy storage, J. Mater. Chem. 6 (2018) 16074–16086.
[82] T. Han, T.X. Fan, S.K. Chow, D. Zhang, Biogenic N-P-codoped TiO2: synthesis, characterization and photocatalytic properties, Bioresour, Technol. 101 (2010) 6829–6835.
[83] M.C. Ortega-Liebana, J.L. Hueso, R. Fernandez-Pacheco, S. Irusta, J. Santamaria, Luminescent mesoporous nanorods as photocatalytic enzyme-like peroxidase surrogates, Chem. Sci. 9 (2018) 7766–7778.
[84] Z.F. Zhu, S.D. Wang, Y.J. Chang, D.B. Yu, Y. Jiang, Direct photodissociation of toluene molecules to photoluminescent carbon dots under pulsed laser irradiation, Carbon 105 (2016) 416–423.
[85] Q. Liu, D.T. Li, Z.F. Zhu, S.M. Yu, Y. Zhang, D.B. Yu, Y. Jiang, N-doped carbon dots from phenol derivatives for excellent colour rendering WLEDs, RSC Adv. 8 (2018) 4850–4856.
[86] A.C. Ferrari, D.M. Basko, Raman spectroscopy as a versatile tool for studying the properties of graphene, Nat. Nanotechnol. 8 (2013) 235–246.
[87] T.Q. Lin, I.W. Chen, F.X. Liu, C.Y. Yang, H. Bi, F.F. Xu, F.Q. Huang, Nitrogen-doped mesoporous carbon of extraordinary capacitance for electrochemical energy storage, Science 350 (2015) 1508–1513.
[88] P. Wu, W. Li, Q. Wu, Y.S. Liu, S.X. Liu, Hydrothermal synthesis of nitrogen-doped carbon quantum dots from microcrystalline cellulose for the detection of Fe^{3+} ions in an acidic environment, RSC Adv. 7 (2017) 44144–44153.
[89] H.Q. Tao, K. Yang, Z. Ma, J.M. Wan, Y.J. Zhang, Z.H. Kang, Z. Liu, In vivo NIR fluorescence imaging, biodistribution, and toxicology of photoluminescent carbon dots produced from carbon nanotubes and graphite, Small 8 (2012) 281–290.
[90] T.H. Yang, L.D. Huang, Y.W. Harn, C.C. Lin, J.K. Chang, C.I. Wu, J.M. Wu, High density unaggregated Au nanoparticles on ZnO nanorod arrays function as efficient and recyclable photocatalysts for environmental purification, Small 9 (2013) 3169–3182.
[91] V. Nguyen, J.H. Si, L.H. Yan, X. Hou, Electron-hole recombination dynamics in carbon nanodots, Carbon 95 (2015) 659–663.
[92] V. Nguyen, J.H. Si, L.H. Yan, X. Hou, Direct demonstration of photoluminescence originated from surface functional groups in carbon nanodots, Carbon 108 (2016) 268–273.
[93] V. Nguyen, L.H. Yan, H.H. Xu, M.M. Yue, One-step synthesis of multi-emission carbon nanodots for ratiometric temperature sensing, Appl. Surf. Sci. 427 (2018) 1118–1123.
[94] S.J. Zhu, Y.B. Song, J. Wang, H. Wan, Y. Zhang, Y. Ning, B. Yang, Photoluminescence mechanism in graphene quantum dots: quantum confinement effect and surface/edge state, Nano Today 13 (2017) 10–14.
[95] Y.P. Sun, B. Zhou, Y. Lin, W. Wang, K.A.S. Fernando, P. Pathak, M.J. Meziani, B.A. Harruff, X. Wang, H.F. Wang, P.J.G. Luo, H. Yang, M.E. Kose, B.L. Chen, L.M. Veca, S.Y. Xie, Quantum-sized carbon dots for bright and colorful photoluminescence, J. Am. Chem. Soc. 128 (2006) 7756–7757.
[96] K.P. Gong, F. Du, Z.H. Xia, M. Durstock, L.M. Dai, Nitrogen-doped carbon nanotube Arrays with high electrocatalytic activity for oxygen reduction, Science 323 (2009) 760–764.
[97] S.Y. Wang, D.S. Yu, L.M. Dai, Polyelectrolyte functionalized carbon nanotubes as efficient metal-free electrocatalysts for oxygen reduction, J. Am. Chem. Soc. 133 (2011) 5182–5185.
[98] L.W. Zhang, H.B. Fu, Y.F. Zhu, Efficient TiO_2 photocatalysts from surface hybridization of TiO_2 particles with graphite-like carbon, Adv. Funct. Mater. 18 (2008) 2180–2189.
[99] S. Banerjee, D.D. Dionysiou, S.C. Pillai, Self-cleaning applications of TiO_2 by photo-induced hydrophilicity and photocatalysis, Appl. Catal. B Environ. 176 (2015) 396–428.
[100] M.O. Valappil, V.K. Pillai, S. Alwarappan, Spotlighting graphene quantum dots and beyond: synthesis, properties and sensing applications, Appl. Mater. Today 9 (2017) 350–371.
[101] B.C.M. Martindale, E. Joliat, C. Bachmann, R. Alberto, E. Reisner, Clean donor oxidation enhances the H-2 evolution activity of a carbon quantum dot-molecular catalyst photosystem, Angew. Chem. Int. Ed. 55 (2016) 9402–9406.
[102] B. Bajorowicz, M.P. Kobylanski, A. Golabiewska, J. Nadolna, A. Zaleska-Medynska, A. Malankowska, Quantum dot-decorated semiconductor micro- and nanoparticles: a review of their synthesis, characterization and application in photocatalysis, Adv. Colloid Interface Sci. 256 (2018) 352–372.
[103] Y. Nosaka, A. Nosaka, Understanding hydroxyl radical ((OH)-O-center dot) generation processes in photocatalysis, ACS Energy Lett. 1 (2016) 356–359.